Thiazolothiazole-Containing Polythiophenes with Low HOMO Level and High Hole Mobility for Polymer Solar Cells

Qinqin Shi, Haijun Fan, Yao Liu, Jianming Chen, Zhigang Shuai, Wenping Hu, Yongfang Li, Xiaowei Zhan

Beijing National Laboratory for Molecular Sciences and Key Laboratory of Organic Solids, Institute of Chemistry, Chinese Academy of Sciences, Beijing 100190, China
Correspondence to: X. Zhan (E-mail: xwzhan@iccas.ac.cn)

Received 30 June 2011; accepted 11 August 2011; published online 12 September 2011
DOI: 10.1002/pola.24938

ABSTRACT: Two regiochemically defined polythiophenes containing thiazolothiazole acceptor unit were synthesized by palladium(0)-catalyzed Stille coupling reaction. The thermal, electrochemical, optical, charge transport, and photovoltaic properties of these copolymers were examined. Compared to **P1** with head-to-head coupling of two middle thiophenes, **P2** with head-to-tail coupling of two middle thiophenes exhibits 40 nm red shift of absorption spectrum in film and 0.3 eV higher HOMO level. Both polymers exhibit field-effect hole mobility as high as 0.02 $cm^2\ V^{-1}\ s^{-1}$. Polymer solar cells (PSCs) were fabricated based on the blend of the polymers and methanofullerene[6,6]-phenyl C71-butyric acid methyl ester ($PC_{71}BM$). The PSC based on **P1**:$PC_{71}BM$ (1:2, w/w) exhibits a power conversion efficiency of 2.7% under AM 1.5, 100 mW cm^{-2}, two times of that based on **P2**:$PC_{71}BM$. The higher efficiency is attributed to lower HOMO (−5.6 eV) and smaller phase separation scale in **P1**:$PC_{71}BM$ blend. Tiny change in thiophene connection of **P1** and **P2** lead to great difference in HOMO, phase separation scale, and efficiency of their photovoltaic devices. © 2011 Wiley Periodicals, Inc. J Polym Sci Part A: Polym Chem 49: 4875–4885, 2011

KEYWORDS: conjugated polymer; field-effect transistor; polymer solar cell; polythiophene; structure–property relations; synthesis; thiazolothiazole

INTRODUCTION Polymer solar cells (PSCs) are promising candidates for low-cost renewable energy sources for their advantages, such as low cost, easy fabrication, lightweight, and the capability to fabricate flexible large-area devices.[1] So far, the most successful PSCs are bulk heterojunction-type (BHJ) devices, which use a blend of electron-rich polymer donor and electron-poor fullerene acceptor, such as methanofullerene [6,6]-phenyl C61-butyric acid methyl ester (PCBM), as the photoactive layer.[2–6] In recent years, power conversion efficiencies (PCEs) of PSCs under simulated sunlight conditions more than 7% have been achieved.[7] Along with the rapid development of polymer materials, the creation of novel donor materials mainly focuses on lowering highest occupied molecular orbita (HOMO) energy level to get high open-circuit voltage (V_{oc}), tuning bandgaps to get broad absorption, and improving the hole mobility.[8–13]

Regioregular poly(3-hexylthiophene) (P3HT) is the most representative donor, and BHJ PSCs based on the P3HT/PCBM system exhibited PCEs of about 5% after device optimization and post-treatments.[14] However, its high HOMO energy level (ca. −4.8 eV) lead to low V_{oc} (ca. 0.6 V), which limited the performance of PSCs.[15] Thus, the electron-withdrawing building blocks,[16–24] such as benzothiadiazole, diketopyrrolo-pyrrole, 2-pyran-4-ylidenemalononitrile, thienopyrazine, thieno[3,4-c]pyrrole-4,6-dione, etc., were introduced into the main chains of polythiophene to afford the D–A copolymers which would lower HOMO level.

Thiazolothiazole has a rigid and coplanar fused ring, and thereby ensures highly extended π-electron system and strong π-stacking. As a result, conjugated small molecules and polymers based on thiazolothiazole exhibited high charge carrier mobilities.[25–27] In particular, McCullough and coworkers[26,27] reported that thiazolothiazole–thiophene copolymers exhibited hole mobilities as high as 0.3 $cm^2\ V^{-1}\ s^{-1}$. Recently, several copolymers of thiazolothiazole with benzodithiophene,[28–30] cyclopentadithiophene,[31] carbazole,[32] and dithienosilole[33] were synthesized for PSC applications, and PCEs up to 5.59% were reported. All these thiazolothiazole-containing photovoltaic polymers are based on fused-ring donor-building blocks other than polythiophene. Moreover, there have been no reports that probe into impact of side chains on absorption, energy levels, and charge transport properties of the thiazolothiazole-containing photovoltaic polymers as well as on morphology and photovoltaic properties of the donor/acceptor blends.

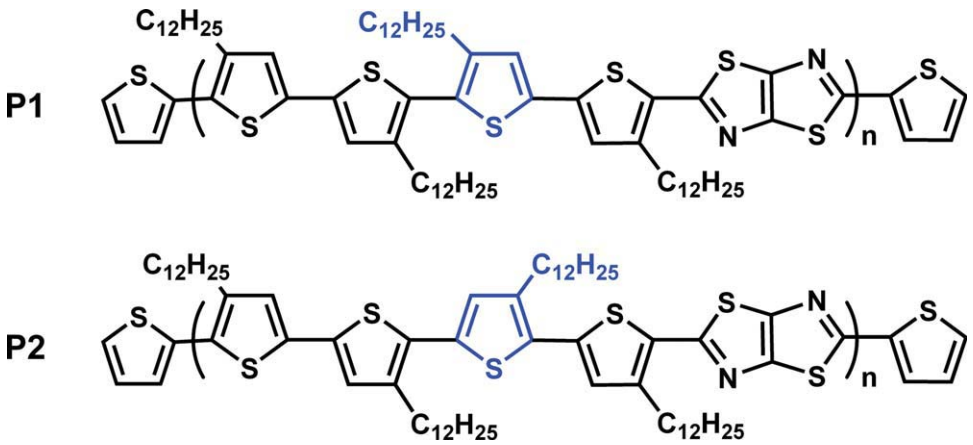

FIGURE 1 Chemical structures of copolymers **P1** and **P2**. [Color figure can be viewed in the online issue, which is available at wileyonlinelibrary.com.]

In this work, we demonstrate synthesis and characterization of two regiochemically defined polythiophenes containing thiazolothiazole acceptor unit (**P1** and **P2**, Fig. 1), which exhibit high hole mobilities (0.02 $cm^2\ V^{-1}\ s^{-1}$) and low HOMO levels (−5.3 to −5.6 eV). Slight difference between **P1** and **P2** lies only on dodecyl position on one thiophene (labeled in blue), while great differences on absorption spectra, HOMO level, blend film morphology, and PCE for their BHJ devices were observed. Although **P2** exhibited a similar hole mobility and red-shifted absorption relative to **P1**, the PSCs based on **P2**/$PC_{71}BM$ blend exhibited PCEs half of that for **P1**/$PC_{71}BM$ (2.7%) due to higher HOMO level and larger phase separation scale.

EXPERIMENTAL

Measurements and Characterization

The ^1H NMR and ^{13}C NMR spectra were measured on a Bruker AVANCE 400 MHz spectrometer using tetramethylsilane ($\delta = 0$ ppm) as an internal standard. Elemental analyses were performed using a FLASH EA1112 elemental analyzer. Thermogravimetric analysis (TGA) measurements were performed using a DTG-60 thermal analysis system under N_2 at a heating rate of 20 °C min^{-1}. Solution (chloroform) and thin-film (on quartz substrate) UV–vis spectra were recorded on a JΛSCO V-570 spectrophotometer. The electrochemical measurements were performed under nitrogen on a deoxygenated solution of tetra-*n*-butylammonium hexafluorophosphate (0.1 M) in acetonitrile with a computer controlled CHI660C electrochemical workstation, a glassy-carbon working electrode, a platinum wire auxiliary electrode, and an Ag wire anodized with AgCl as a pseudo-reference electrode. Potentials were referenced to the ferrocenium/ferrocene ($FeCp_2^{+/0}$) couple using ferrocene as an internal standard. The gel permeation chromatography (GPC) measurements were performed on a Waters 515 chromatograph connected to a Waters 2410 refractive index detector, using THF as eluent and polystyrene standards as calibrants, three Waters Styragel columns (HT3, 5, 6E) connected in series were used. X-ray diffraction (XRD) pattern of thin films was performed in the reflection mode at 40 kV and 200 mA with Cu Kα radiation using a 2 kW Rigaku D/max-2500 X-ray diffractometer. The morphology of blend films was observed by an atomic force microscopy (AFM; NanoMan VS, Veeco) in contact mode.

OFET Device Fabrication and Characterization

Field-effect transistors based on **P1** or **P2** polymer films were fabricated in a bottom gate, top contact configuration at ambient atmosphere. Highly *n*-doped silicon and thermally grown silicon dioxide (300 nm) were used as back gate and gate dielectric, respectively. The substrate were cleaned with pure water, hot concentrated sulfuric acid-hydrogen peroxide solution (concentrated sulfuric acid/hydrogen peroxide water = 2:1), pure water, and pure isopropanol. Then vaporized octadecyltrichlorosilane (OTS) was used for surface modification of the gate dielectric layer.

Solutions of the polymers in *o*-dichlorobenzene (about 5 mg mL^{-1}) were spin coated on hot OTS treated substrates (about 80 °C) to form thin films. Before thermal evaporation of top contacts, the films were baked at 120 °C in a vacuum chamber for 30 min to remove the residual solvent. Gold contacts (25 nm) for source and drain electrodes (finger parallel source–drain geometry) were vacuum-deposited at a rate of 0.1 Å s^{-1} through a metal shadow mask that defined a series of transistor devices with a channel length (L) of 50 μm and a channel width (W) of 1 mm. The characterization was accomplished by Keithley 4200 SCS with a micromanipulator 6150 probe station in a clean shielded box at ambient atmosphere. Then field-effect mobility was calculated from the standard equation for saturation region in metal-dioxide-semiconductor field-effect transistors: $I_{DS} = (W/2L)\mu C_i(V_G\text{-}V_T)^2$, where I_{DS} is the drain–source current, μ is the field-effect mobility, W and L are the channel width and length, C_i is the capacitance per unit area of the dielectric layer ($C_i = 9.6$ nF cm^{-2}), V_G is the gate voltage and V_T is the threshold voltage.

PSC Device Fabrication and Characterization

The PSC devices were fabricated with a structure of ITO/PEDOT:PSS/**P1(P2)**:$PC_{71}BM$/Al. The patterned ITO glass

(sheet resistance = 30 Ω $\square^{-1}$) was precleaned in an ultrasonic bath of acetone and isopropanol, and treated in ultraviolet-ozone chamber (Jelight Company, USA) for 30 min. A thin layer (30 nm) of poly(3,4-ethylenedioxythiophene):poly(styrene sulfonate) (PEDOT:PSS, Baytron P VP AI 4083, Germany) was spin-coated onto the ITO glass and baked at 150 °C for 30 min. A chlorobenzene solution of blend of **P1** or **P2**/$PC_{71}BM$ (1:1 or 1:2, w/w) was subsequently spin-coated on the surface of PEDOT:PSS layer to form a photosensitive layer. An aluminium layer (ca. 60 nm) was then evaporated onto the surface of the photosensitive layer under vacuum (ca. 10^{-4} Pa) to form the cathode. The active area of the device was 4 mm^2. Current–voltage curve was measured with a computer-controlled Keithley 236 Source Measure Unit. A xenon lamp coupled with AM 1.5 solar spectrum filters was used as the light source, and the optical power at the sample was 100 mW cm^{-2}. The incident photon-to-current conversion efficiency (IPCE) spectrum was measured by Stanford Research Systems model SR830 DSP lock-in amplifier coupled with WDG3 monochromator and 500 W xenon lamp.

Materials

3,3′-Didodecyl-2,2′-bithiophene,[34] 2,5-bis(5-bromo-3-dodecyl thiophen-2-yl)-thiazolo[5,4-*d*]thiazole,[27] 2,5-bis(5-trimethylstannane-3-dodecyl thiophen-2-yl)-thiazolo[5,4-*d*]thiazole,[27] and 5,5′-dibromo-3,4′-didodecyl-2,2′-bithiophene[35] were synthesized according to the literature methods. Toluene and tetrahydrofuran (THF) were distilled from sodium benzophenone under nitrogen before use. Bio-Rad Bio-Beads S-X1 is a kind of porous crosslinked polystyrene polymers used for gel permeation separations of lipophilic polymers and low molecular weight, hydrophobic materials in the presence of organic solvents. Unless stated otherwise, the other reagents were purchased from commercial sources, and used without further purification.

(3,3′-Didodecyl-2,2′-bithiophene-5,5′-diyl)bis(trimethylstannane)

To a solution of 3,3′-didodecyl-2,2′-bithiophene (251 mg, 0.5 mmol) in 8 mL of THF was added dropwise a 2.5 M solution of *n*-butyllithium in hexane (0.8 mL, 2 mmol) at −78 °C. The solution was stirred at −78 °C for 30 min and at room temperature for another 1 h. The solution was then cooled to −78 °C, and trimethyltin chloride (300 mg, 1.5 mmol) was added in one portion. The solution was warmed to room temperature and 30 mL of water and 30 mL of diethyl ether were added. The organic layer was washed twice with 30 mL of water and dried over magnesium sulfate. After filtration, the solvent was removed from the filtrate *in vacuo* to yield the product as a colorless oil (370 mg, 90%). ^{1}H NMR (400 MHz, $CDCl_3$): δ 7.02 (s, 2H), 2.51 (t, J = 7.9 Hz, 4H), 1.26–1.24 (m, 40H), 0.88 (t, J = 6.7 Hz, 6H), 0.38 (s, 18H). ^{13}C NMR (100 MHz, $CDCl_3$): d 142.88, 137.34, 136.87, 135.25, 32.02, 31.02, 30.83, 30.06, 29.76, 29.67, 29.57, 29.53, 29.45, 28.82, 22.78, 14.20, −8.20.

Poly{(3,3′-didodecyl-2,2′-bithiophene-5,5′-diyl)-alt-[2,5-bis (3-dodecyl-thiophen-2-yl)thiazolothiazole-5,5′-diyl]} (P1)

2,5-Bis(5-bromo-3-dodecylthiophen-2-yl)-thiazolo[5,4-*d*]thiazole (80 mg, 0.1 mmol) and (3,3′-didodecyl-2,2′-bithiophene-5,5′-diyl)bis(trimethylstannane) (83 mg, 0.1 mmol) were dissolved in 10 mL of anhydrous toluene and deoxygenated with N_2 for 30 min. $Pd(PPh_3)_4$ (11.5 mg, 0.01 mmol) was then added under N_2. The mixture was stirred at reflux for 3 days. To end-cap the polymer chain, tributyl(thiophen-2-yl)stannane (3.7 mg, 0.01 mmol) was added under nitrogen and the mixture was stirred at reflux for 10 h. 2-Bromothiophene (3.3 mg, 0.02 mmol) was then added under nitrogen, and the mixture was stirred at reflux for 10 h. After the reaction mixture was cooled to room temperature, the polymer was precipitated by addition of 80 mL of methanol. The precipitate was filtered. Finally, the polymer was purified by size exclusion column chromatography over Bio-Rad Bio-Beads S-X1 eluting with chloroform. The polymer was recovered as a purple solid from the chloroform fraction by rotary evaporation (80 mg, 70%). ^{1}H NMR (400 MHz, $CDCl_3$): δ 7.09–6.91 (br, 4H), 2.93 (br, 4H), 2.55 (br, 4H), 1.75–1.26 (br, 80H), 0.85 (br, 12H). GPC: M_n 10,659; M_w 38,986; M_w/M_n 3.66. Anal. Calcd for $(C_{68}H_{104}N_2S_6)_n$: C, 71.52; H, 9.18; N, 2.45. Found: C, 66.80; H, 9.08; N, 2.31%.

Poly{(3,4′-didodecyl-2,2′-bithiophene-5,5′-diyl)-alt-[2,5-bis (3-dodecyl-thiophen-2-yl)thiazolothiazole-5,5′-diyl]} (P2)

2,5-Bis(3-dodecyl-5-trimethylstannyl-thiophen-2-yl)-thiazolo[5,4-*d*]thiazole (97 mg, 0.1 mmol) and 5,5′-dibromo-3,4′-didodecyl-2,2′-bithiophene (66 mg, 0.1 mmol) were dissolved in 10 mL of anhydrous toluene and deoxygenated with N_2 for 30 min. $Pd(PPh_3)_4$ (11.5 mg, 0.01 mmol) was then added under N_2. The mixture was stirred at reflux for 3 days. To end-cap the polymer chain, tributyl(thiophen-2-yl)stannane (3.7 mg, 0.01 mmol) was added under nitrogen and the mixture was stirred at reflux for 10 h. 2-Bromothiophene (3.3 mg, 0.02 mmol) was then added under nitrogen, and the mixture was stirred at reflux for 10 h. After the reaction mixture was cooled to room temperature, the polymer was precipitated by addition of 80 mL of methanol. The precipitate was filtered. Finally, the polymer was purified by size exclusion column chromatography over Bio-Rad Bio-Beads S-X1 eluting with chloroform. The polymer was recovered as a purple solid from the chloroform fraction by rotary evaporation (80 mg, 70%). ^{1}H NMR (400 MHz, $CDCl_3$): δ 7.02 (br, 4H), 2.92 (br, 8H), 1.73–1.26 (br, 80H), 0.87 (br, 12H). GPC: M_n 14,816; M_w 74,397; M_w/M_n 5.02. Anal. Calcd for $(C_{68}H_{104}N_2S_6)_n$: C, 71.52; H, 9.18; N, 2.45. Found: C, 68.73; H, 8.64; N, 2.38%.

RESULTS AND DISCUSSION

Synthesis and Characterization

Scheme 1 shows the synthetic routes to the monomer and copolymers. Copolymerization was performed by Stille coupling reaction using $Pd(PPh_3)_4$ as catalyst in toluene. The polymers were purified by size exclusion column chromatography over Bio-Rad Bio-Beads S-X1 eluting with chloroform.

Molecular weights of the polymers were determined by GPC using polystyrene standards as calibrants (Table 1). **P1** has a number-average molecular weight (M_n) of 10,659 with polydispersity index (M_w/M_n) of 3.66; **P2** has a M_n of 14,816 with M_w/M_n of 5.02. These number-average molecular

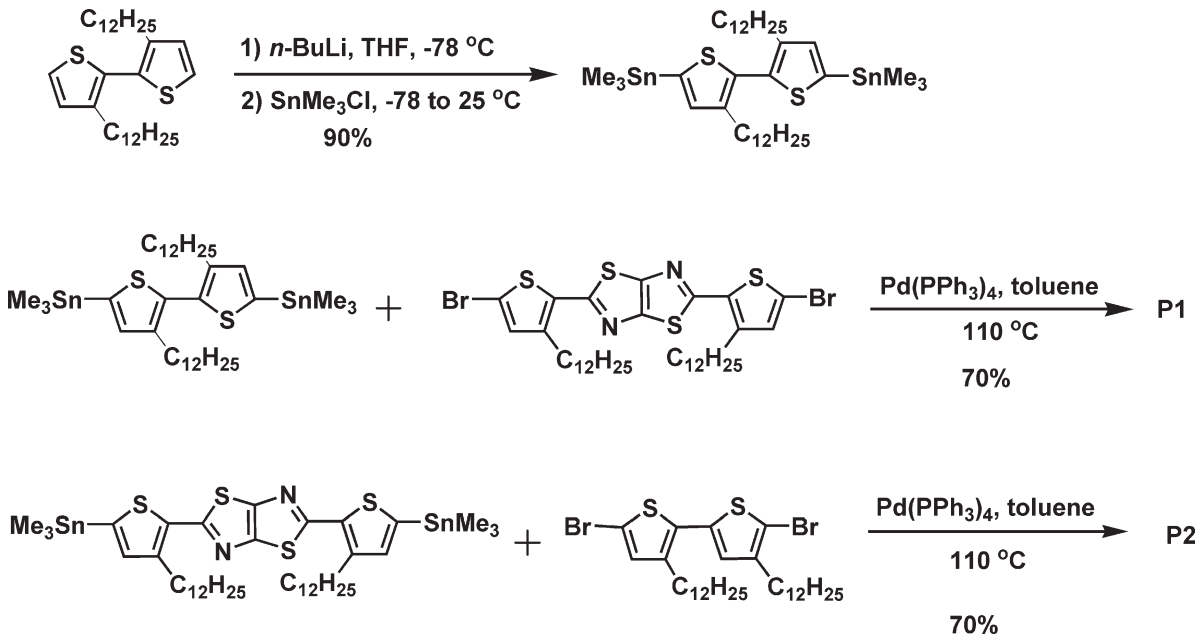

SCHEME 1 Synthetic routes of the polymers.

weights are larger than that (4100–8700) reported for a similar thiazolothiazole–thiophene copolymers.[26] **P1** and **P2** are soluble in common organic solvents, such as chloroform, THF, and chlorobenzene. Both polymers show good thermal stability with decomposition temperatures over 340 °C, as measured by TGA (Fig. 2).

Theory Calculation

We use density functional theory (DFT) at the B3LYP/6-31G (d, p) level[36,37] with Gaussian 09 program package[38] to provide an insight into the molecular architecture of the polymers. Here, the molecular simulation was performed for **P1** and **P2** with a chain length of $n = 1$. Dihedral angles between thiophenes (D_1, D_2, and D_3; Fig. 3) are susceptible to the position of dodecyl on thiophene. In particular, the dihedral angle (D_2) between two middle thiophenes in **P1** is 64°, much larger than that (−18.1°) in **P2**. The dihedral angles in **P1** and **P2** show the same trend reported in the literature.[39] Thus, **P1** has a more twisted main chain, whereas **P2** has a more coplanar main chain. The planar conformation of the main chain leads to strong interchain interaction in **P2**.

TABLE 1 Molecular Weights and Thermal Data of Copolymers **P1** and **P2**

Polymer	Yield (%)	M_n[a]	M_w[a]	M_w/M_n[a]	T_d[b] (°C)
P1	70	10659	38986	3.66	349
P2	70	14816	74397	5.02	370

[a] Number-average molecular weight (M_n), weight-average molecular weight (M_w), and polydispersity index (M_w/M_n) were measured by GPC using THF as an eluent and polystyrene as a standard.
[b] Temperature at 5% weight loss measured by TGA at a heating rate of 20 °C min^{-1} under nitrogen.

Figure 4 shows the calculated molecular orbital geometry and energy levels of the polymers. For **P1** and **P2**, the HOMOs are delocalized over the polymer backbones. The lowest unoccupied molecular orbital (LUMO) in **P1** is located on thiazolothiazole and adjacent bithiophene unit, whereas the LUMO in **P2** is delocalized over the polymer backbone. Relative to **P2**, **P1** has a lower HOMO and a slightly higher LUMO because of the twisted main chain and relatively localized HOMO and LUMO.

Optical Properties

The normalized spectra of optical absorption of the copolymers in chloroform solution (10^{-6} M) and solid film are shown in Figure 5. The absorption maxima for **P1** and **P2** in chloroform are 484 and 500 nm, respectively (Table 2). As a

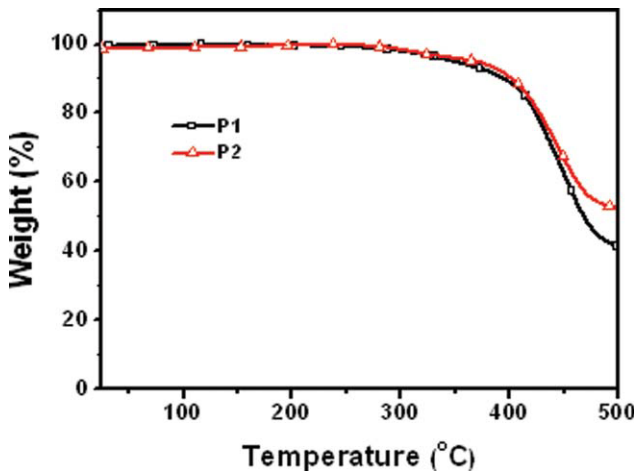

FIGURE 2 TGA curves of polymers **P1** and **P2**. [Color figure can be viewed in the online issue, which is available at wileyonlinelibrary.com.]

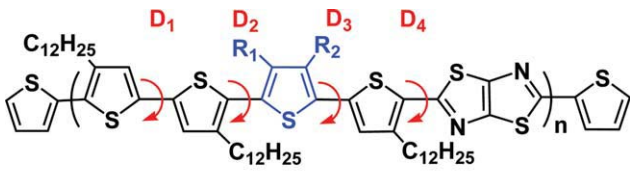

	R_1	R_2	D_1	D_2	D_3	D_4
P1	$C_{12}H_{25}$	H	-13.8	64.0	-6.5	-1.3
P2	H	$C_{12}H_{25}$	6.61	-18.1	19.8	-1.6

FIGURE 3 Several key dihedral angles of the polymers. [Color figure can be viewed in the online issue, which is available at wileyonlinelibrary.com.]

result of the more twisted structure of main chain[40] and low molecular weight,[41] polymer **P1** exhibits blue-shifted absorption relative to **P2**. The absorption maximum of **P1** and **P2** in solid films red shifts 36 and 60 nm relative to that in solution, respectively, which can be attributed to the strong π–π interchain association and aggregation. Although higher molecular weight could improve conjugation length to a certain extent, the significant red shift of absorption for **P2** in solid film mainly benefits from more planar conformation of the polymer backbone, which extends the conjugation length of the π electrons and causes stronger interchain interaction. The optical bandgaps estimated from the absorption edge of **P1** and **P2** are 1.91 and 1.85 eV, respectively.

Electrochemical Properties

Figure 6 shows the cyclic voltammetry curves of the studied polymers using polymer film on glassy carbon working electrode in 0.1 M Bu_4NPF_6 acetonitrile solution at a potential scan rate of 50 mV s^{-1}. Apparently, they show a similar profile with one quasi-reversible oxidation peak and one irreversible reduction peak. The HOMO and LUMO values of **P1** and **P2** are estimated from the onset oxidation and reduction potentials, assuming the absolute energy level of $FeCp_2^{+/0}$ to be 4.8 eV below vacuum (Table 3).[42] Because of the incomplete reversibility of these processes, the peaks do not necessarily represent the thermodynamic oxidation and reduction potentials and should be interpreted with caution. However,

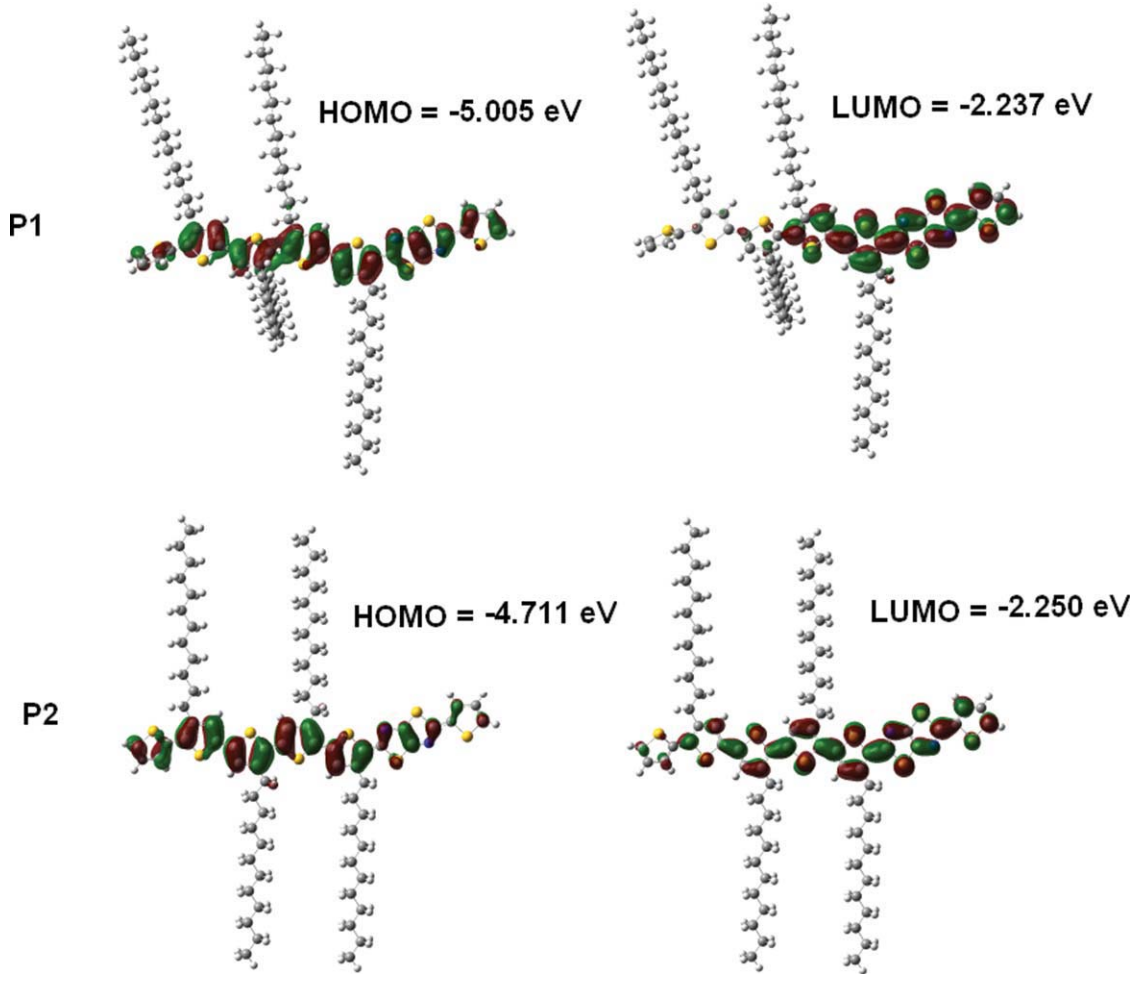

FIGURE 4 Molecular orbital geometry and energy levels obtained from DFT calculations on **P1** and **P2** with a chain length $n = 1$ at B3LYP/6-31G* level. [Color figure can be viewed in the online issue, which is available at wileyonlinelibrary.com.]

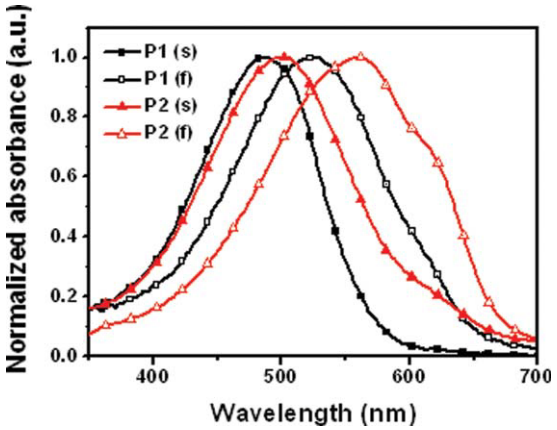

FIGURE 5 Absorption spectra of **P1** and **P2** in chloroform (s) and in thin film (f). [Color figure can be viewed in the online issue, which is available at wileyonlinelibrary.com.]

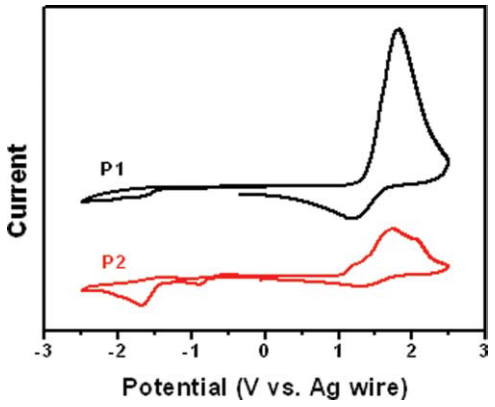

FIGURE 6 Cyclic voltammograms for **P1** and **P2** in CH_3CN/0.1 M $[Bu_4N]^+[PF_6]^-$ at 50 mV s^{-1}. [Color figure can be viewed in the online issue, which is available at wileyonlinelibrary.com.]

the electrochemical data do reveal an interesting trend: **P2** with a more planar main chain has a higher HOMO and a slightly lower LUMO. The trends in the electrochemical data are therefore consistent with the trends in the absorption maxima and theory calculation. Polymer **P2** has a more coplanar backbone; the π-electrons are more delocalized. Moreover, the higher molecular weight of **P2** extends conjugation length and lowers the bandgap. Accordingly, polymer **P2** is easier to oxidize and has a smaller bandgap.[43,44] It is worthy noting that **P1** has a low HOMO (−5.60 eV), 0.8 eV lower than that of P3HT (ca. −4.8 eV)[15] due to the electron-withdrawing unit thiazolo[5,4-*d*]thiazole and twisted main chain. The difference between the LUMO (−3.9 eV[45,46]) of the acceptor $PC_{71}BM$ and the HOMO of the donor **P1** is as large as 1.7 eV, which could lead to high open-circuit voltage (V_{oc}) of solar cells.

Organic Field-Effect Transistors

To ensure effective charge carrier transport to the electrodes and reduce the photocurrent loss in solar cells, the high hole mobility is a basic requirement for effective photovoltaic polymer donors. To measure hole mobilities of the polymers, organic field-effect transistors (OFETs) based on **P1** and **P2** were fabricated on OTS-treated SiO_2/Si substrates through spin-coating process. In a top contact geometry using Au as the source and drain electrodes, both polymers exhibited typical p-type semiconductor behavior in air. The p-type output curve and the corresponding transfer characteristics are depicted in Figure 7, which exhibits good current modulation and well-defined linear and saturation regions. The highest hole mobility of all the devices based on **P1** and **P2** in air are 0.02 cm^2 V^{-1} s^{-1} with current on/off ratio of 10^4 (Table 4). The hole mobilities of **P1** and **P2** are among the top values reported for photovoltaic polymers.[8] In general, for same polymer, a higher molecular weight leads to a higher mobility. However, **P2** has a higher molecular weight than **P1**, whereas the mobility of **P2** is same as that for **P1**. This result indicates that the difference in charge transport does not originate from the difference in molecular weights of **P1** and **P2**.

Thin films of **P1** and **P2** on OTS-modified Si/SiO_2 substrates were investigated by XRD patterns. Figure 8 shows the XRD patterns of **P1** and **P2**. No reflection peaks are observed in $2\theta < 10^\circ$ region for **P1** and **P2** thin films, indicating that the **P1** and **P2** thin films are amorphous. The slight difference in XRD patterns of **P1** and **P2** thin films is a weak broad peak accompanied with a weak sharp peak appeared at $2\theta = 21^\circ$ corresponding to a distance of 4.2 Å in **P1**, indicating somewhat ordered and π–π stacking structures. Figure 9 shows the AFM height images of **P1** and **P2** thin films. The **P2** film are more smooth and flat with a smaller root-mean-square (RMS) surface roughness of about 0.64 nm than **P1** film (RMS roughness of about 1.89 nm) probably because of its higher molecular weight. The balance between the more ordered π–π stacking structure of **P1** and more smooth morphology of **P2** thin films leads to a similar mobilities.

TABLE 2 Absorption Data of **P1** and **P2**

	$\lambda_{max}^{abs\ a}$ (nm)		
Polymer	Solution	Film	$E_g^{opt\ b}$ (eV)
P1	484	520	1.91
P2	500	560	1.85

[a] Absorption maxima.
[b] Optical bandgap estimated from the onset edge of absorption spectra in solid film.

TABLE 3 Redox Potentials and Energy Levels of the Polymers[a]

	E_{ox}^{b} (V)	E_{red}^{b} (V)	HOMO[c] (eV)	LUMO[c] (eV)
P1	+0.80	−2.05	−5.60	−2.75
P2	+0.50	−2.01	−5.30	−2.79

[a] Polymer thin films on glassy-carbon electrode in CH_3CN/0.1 M $[Bu_4N]^+[PF_6]^-$ at 50 mV s^{-1}.
[b] E_{ox} is the onset potentials versus ferrocenium/ferrocene corresponding to oxidation, whereas E_{red} is the onset potentials versus ferrocenium/ferrocene corresponding to reduction.
[c] HOMOs and LUMOs estimated from the onset oxidation and reduction potentials, respectively, assuming the absolute energy level of ferrocene/ferrocenium to be 4.8 eV below vacuum.

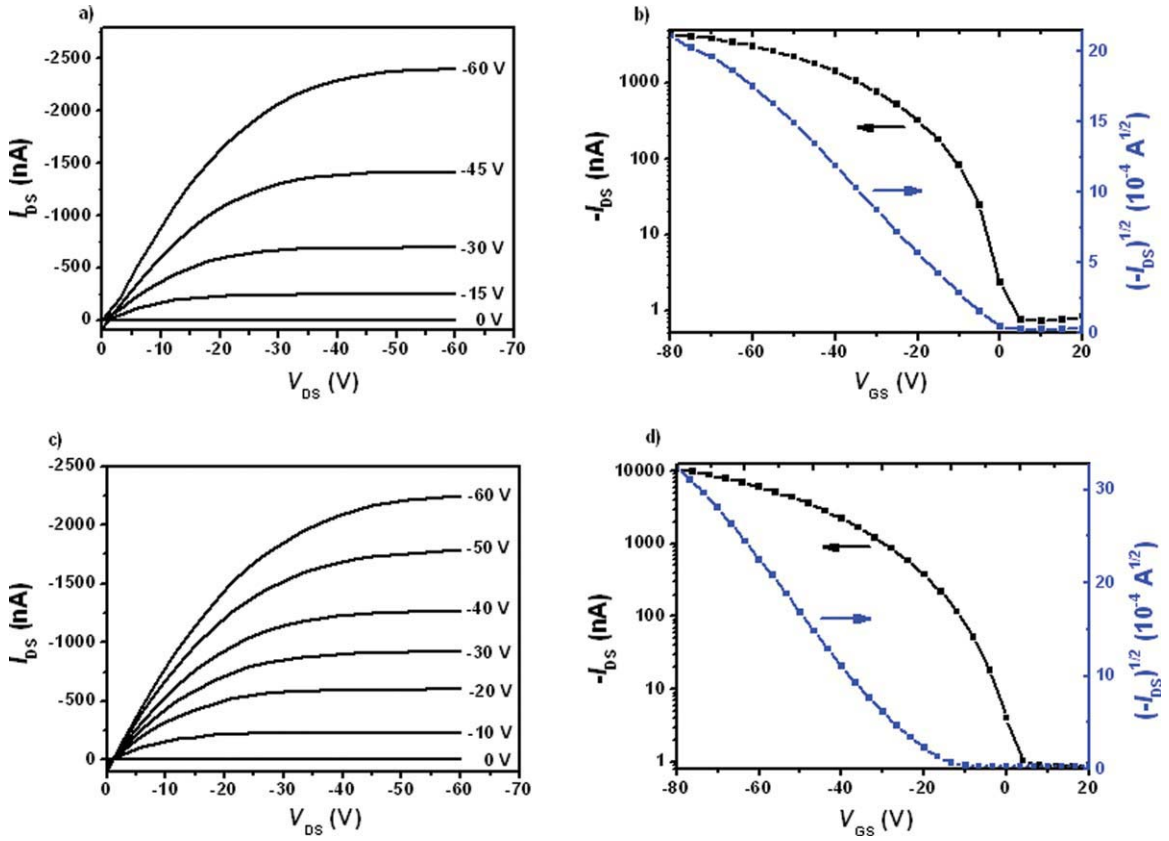

FIGURE 7 Typical current–voltage characteristics (I_{DS} vs. V_{DS}) at different gate voltages (V_{GS}), and $-I_{DS}$ and $(-I_{DS})^{1/2}$ vs. V_{GS} plots at V_{DS} of −100 V for a top contact device based on **P1** (a, b) and **P2** (c, d). [Color figure can be viewed in the online issue, which is available at wileyonlinelibrary.com.]

TABLE 4 OFET Characteristics of **P1** and **P2** in Air

Polymer	μ_h (cm^2 V^{-1} s^{-1})	I_{on}/I_{off}	V_{th} (V)
P1	0.02	10^4	−1.1
P2	0.02	10^4	−10

Photovoltaic Properties

Because of broad absorption, low HOMO levels, and high hole mobilities of **P1** and **P2**, we investigated the potential of the polymers for photovoltaic applications. We used **P1** and **P2** as an electron donor and soluble fullerene derivative $PC_{71}BM$ as an electron acceptor,[47] and fabricated bulk heterojunction PSCs with a structure of ITO/PEDOT:PSS/**P1**(**P2**):$PC_{71}BM$/Al. Figure 10 shows current density–voltage

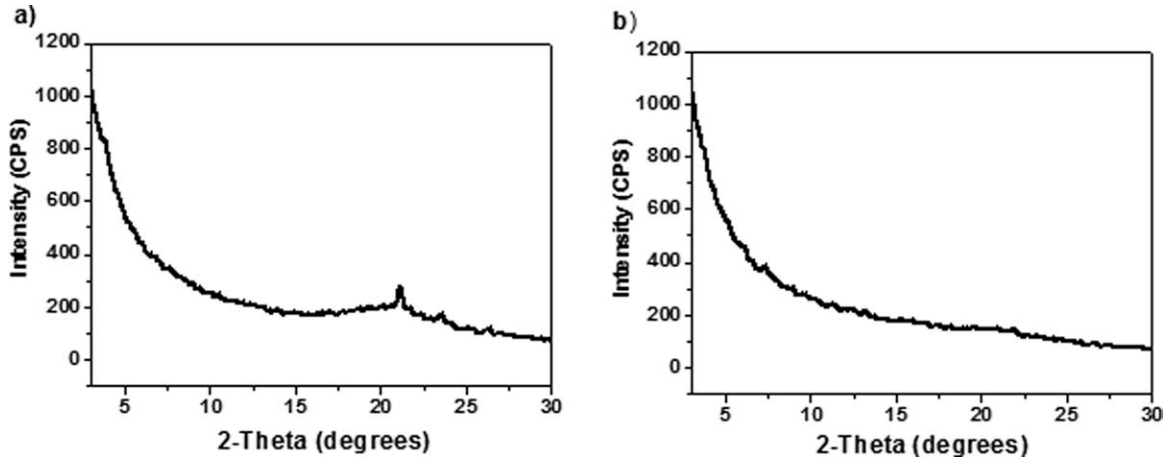

FIGURE 8 XRD patterns of thin films of **P1** (a) and **P2** (b) on OTS-modified Si/SiO_2 substrates.

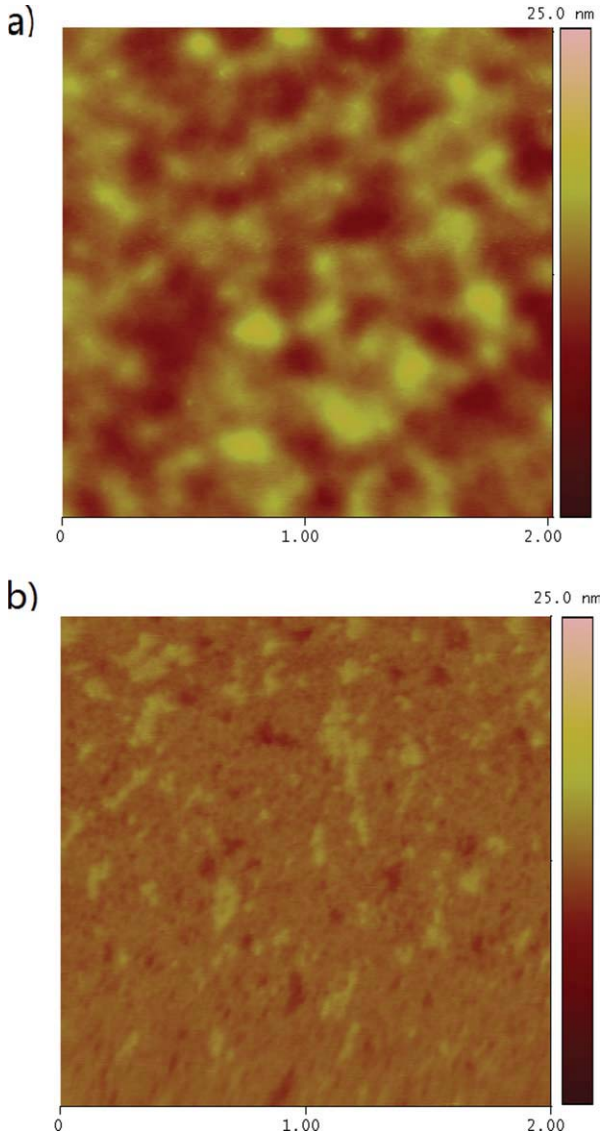

FIGURE 9 AFM topographic (2×2 μm^2) images of thin films of **P1** (a) and **P2** (b) on OTS-modified Si/SiO_2 substrates. [Color figure can be viewed in the online issue, which is available at wileyonlinelibrary.com.]

characteristics and IPCE as a function of wavelength of a device with the structure ITO/PEDOT:PSS/**P1**(**P2**):$PC_{71}BM$ (1:2, w/w)/Al. Table 5 shows the open-circuit voltage (V_{oc}), short-circuit current density (J_{sc}), fill factor (FF), and PCE of devices with different weight ratios in the active blend layers. The weight ratio of **P1**:$PC_{71}BM$ strongly affects FF, but slightly affects V_{oc} and J_{sc}. When **P1**:$PC_{71}BM$ weight ratio was 1:2, the device gave a better photovoltaic performance; V_{oc}, J_{sc}, FF, and PCE of **P1** device was 0.93 V, 5.94 mA cm^{-2}, 48.9% and 2.70%, respectively. Similarly, the weight ratio of **P2**:$PC_{71}BM$ affects J_{sc} and FF more significantly than V_{oc}. When **P2**:$PC_{71}BM$ weight ratio was 1:2, the device gave a better photovoltaic performance; V_{oc}, J_{sc}, FF, and PCE of **P2** device was 0.82 V, 4.49 mA cm^{-2}, 36.1% and 1.33%, respectively. The higher V_{oc} of **P1**-based device benefits from lower HOMO of **P1**.

As shown in Figure 10, although **P1**(**P2**):$PC_{71}BM$ had a similar broad absorption plateau between 300 and 700 nm, IPCE values of **P1** were generally 10% higher than that of **P2**, lead to higher J_{sc} of **P1**. Different J_{sc} generally involves three

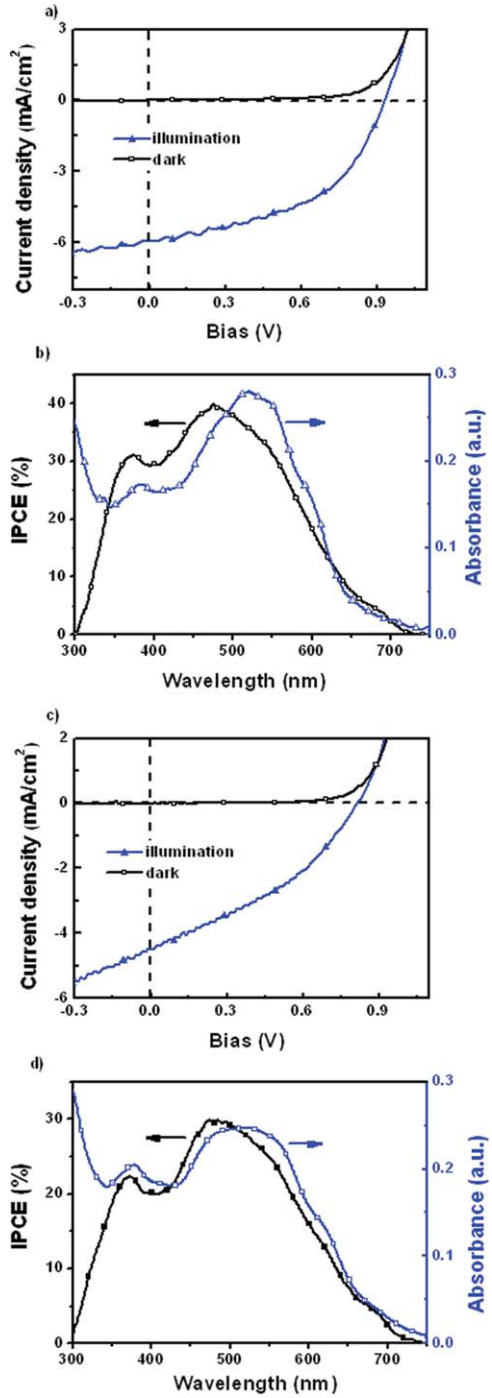

FIGURE 10 Current density–voltage characteristics of a device with the structure ITO/PEDOT:PSS/**P1**(**P2**):$PC_{71}BM$ [1:2, w/w)/Al (a): **P1**; (c): **P2**] and absorption spectrum of a film of **P1**(**P2**):$PC_{71}BM$ (1:2, w/w) blend and IPCE as a function of wavelength under the illumination of an AM 1.5 solar simulator, 100 mW cm^{-2} (b): **P1**; and (d): **P2**). [Color figure can be viewed in the online issue, which is available at wileyonlinelibrary.com.]

TABLE 5 Photovoltaic Performance of PSCs Based on **P1** and **P2** Under the Illumination of AM 1.5, 100 mW cm^{-2}

Active layer	V_{oc} (V)	J_{sc} (mA cm^{-2})	FF (%)	PCE (%)
P1:$PC_{71}BM$ = 1:1	0.94	5.61	30.4	1.60
P1:$PC_{71}BM$ = 1:2	0.93	5.94	48.9	2.70
P2:$PC_{71}BM$ = 1:1	0.81	4.02	33.5	1.09
P2:$PC_{71}BM$ = 1:2	0.82	4.49	36.1	1.33

processes in BHJ solar cells, namely the generation of excitons, the diffusion of excitons to the donor/acceptor interfaces, and the transport of separated free charges to the electrodes. The generation of exciton is closely related to the absorption of the active layers. Because of similar absorption spectra of the **P1**(**P2**):$PC_{71}BM$ blend, the generation of exciton in the blends is similar and does not cause big difference of J_{sc}. Therefore, the main origin for different J_{sc} is the exciton diffusion and charge transport, which are closely related to the phase separation state. Larger donor/acceptor interfaces, which facilitate the diffusion and separation of excitons, and charge transport, could be achieved by reducing the phase separation scale. An ideal nanoscale phase separation of less than 20 nm was recommended based on the consideration of the short exciton diffusion length of less than 10 nm in BHJ devices.[48,49] Figure 11 shows the actual phase separation state of blend films of **P1**(**P2**):$PC_{71}BM$. **P1**:$PC_{71}BM$ blend film is smooth and flat with a RMS roughness of 0.42 nm, whereas **P2**:$PC_{71}BM$ blend film gives coarser surface with a RMS of 1.02 nm. From the phase image of **P2**:$PC_{71}BM$ [Fig. 9(d)], the distinct phase separation with domain size of about 50 nm was observed. This large phase separation scale is not favorable for efficient exciton dissociation, lead to lower J_{sc}. Moreover, the lower FF in **P2**-based device is also attributed to coarse morphology and large phase separation. In comparison with **P1**, the head-to-tail coupling of two middle thiophenes in polymer **P2** endows the main chain with more planar structure, which is supported by theory calculation, absorption, and electrochemistry data. The more planar backbone of **P2** favors stronger π–π interchain interaction and stronger aggregation in the thin film, lead to coarse morphology and large phase separation when blending with $PC_{71}BM$. In general, for same polymer donor, a higher molecular weight leads to a higher PCE when blending with fullerene acceptor.[41,50] However, **P2** has a higher molecular weight than **P1**, whereas the PCE of PSCs based on **P2**/$PC_{71}BM$ blend is only half of that for **P1**/$PC_{71}BM$ device. This result indicates that the difference in photovoltaic properties does not originate from the difference in molecular weights of **P1** and **P2**.

CONCLUSIONS

Two regiochemically defined polythiophenes containing thiazolothiazole acceptor unit, **P1** and **P2**, have been synthesized. They exhibit high hole mobilities and low HOMO levels. Slight difference between them lies only on the connection of two middle thiophenes, whereas great differences on absorption spectra, HOMO level, blend film morphology, and PCE for their BHJ devices were observed. In comparison with **P1** with head-to-head coupling of two middle thiophenes, the head-to-tail coupling of two middle thiophenes in polymer **P2** endows the main chain with smaller torsion angle and more planar structure. The π-electrons in

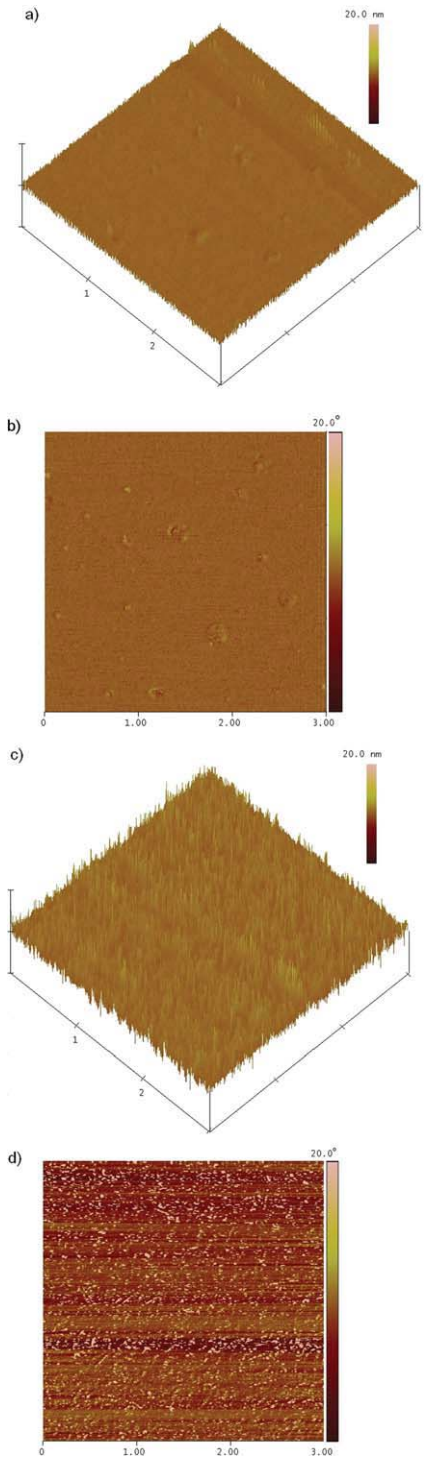

FIGURE 11 AFM topographic (3 × 3 μm^2) (a and c) and phase images (b and d) for thin films of **P1**(**P2**):$PC_{71}BM$ (1:2, w/w) blend (a) and (b): **P1**; (c) and (d): **P2**.

P2 are more delocalized. Accordingly, the polymer is easier to oxidize and has a higher HOMO level and a smaller bandgap, lead to red shift of absorption spectra. The more planar backbone of **P2** favors stronger π–π interchain interaction and stronger aggregation in the thin film, lead to significant red shift of absorption spectra in thin film relative to that in solution. Moreover, the strong aggregation of **P2** in solid state leads to coarse morphology and large phase separation scale in film of **P2**/$PC_{71}BM$ blend. This large phase separation scale is not favorable for efficient diffusion and separation of excitons, lead to lower J_{sc} and lower FF. The PSCs based on **P1**/$PC_{71}BM$ (1:2, w/w) show PCE of 2.70% with V_{oc} of 0.93 V, J_{sc} of 5.94 mA/cm^2 and FF of 48.9%, whereas the PSCs based on **P2**/$PC_{71}BM$ (1:2, w/w) blend exhibit PCE of 1.33%, which is only half of that for **P1**/$PC_{71}BM$ device although **P2** exhibited a higher molecular weight, a similar hole mobility and red-shifted absorption. Although the PCEs achieved here are not competitive with other copolymers of thiazolothiazole with benzodithiophene,[30] carbazole,[32] and dithienosilole,[33] this work nonetheless demonstrates thiazolothiazole-containing polythiophenes as potential photovoltaic materials and an effective way to tune phase separation scale and key parameters, such as V_{oc}, J_{sc}, FF, and PCE, in PSCs by simple chemical modification (changing counit connection).

This work was supported by NSFC (Grants 21025418, 51011130028, 21021091), 973 Project (Grant 2011CB808400), and the Chinese Academy of Sciences.

REFERENCES AND NOTES

1 Arias, A. C.; MacKenzie, J. D.; McCulloch, I.; Rivnay, J.; Salleo, A. Chem Rev 2010, 110, 3–24.

2 Cravino, A. Polym Int 2007, 56, 943–956.

3 Roncali, J. Chem Soc Rev 2005, 34, 483–495.

4 Coakley, K. M.; McGehee, M. D. Chem Mater 2004, 16, 4533–4542.

5 Gunes, S.; Neugebauer, H.; Sariciftci, N. S. Chem Rev 2007, 107, 1324–1338.

6 Winder, C.; Sariciftci, N. S. J Mater Chem 2004, 14, 1077–1086.

7 Chen, H. Y.; Hou, J. H.; Zhang, S. Q.; Liang, Y. Y.; Yang, G. W.; Yang, Y.; Yu, L. P.; Wu, Y.; Li, G. Nat Photon 2009, 3, 649–653.

8 Zhan, X. W.; Zhu, D. B. Polym Chem 2010, 1, 409–419.

9 Osaka, I.; McCullough, R. D. Acc Chem Res 2008, 41, 1202–1214.

10 Bundgaard, E.; Krebs, F. C. Sol Energ Mater Sol Cells 2007, 91, 954–985.

11 Chen, J. W.; Cao, Y. Acc Chem Res 2009, 42, 1709–1718.

12 Li, Y. F.; Zou, Y. P. Adv Mater 2008, 20, 2952–2958.

13 Cheng, Y. J.; Yang, S. H.; Hsu, C. S. Chem Rev 2009, 109, 5868–5923.

14 Li, G.; Shrotriva, V.; Huang, J. S.; Yao, Y.; Moriarty, T.; Emery, K.; Yang, Y. Nat Mater 2005, 4, 864–868.

15 Hou, J. H.; Tan, Z. A.; Yan, Y.; He, Y. J.; Yang, C. H.; Li, Y. F. J Am Chem Soc 2006, 128, 4911–4916.

16 Beaujuge, P. M.; Subbiah, J.; Choudhury, K. R.; Ellinger, S.; McCarley, T. D.; So, F.; Reynolds, J. R. Chem Mater 2010, 22, 2093–2106.

17 Wienk, M. M.; Turbiez, M.; Gilot, J.; Janssen, R. A. J. Adv Mater 2008, 20, 2556–2560.

18 Li, Y. W.; Xue, L. L.; Li, H.; Li, Z. F.; Xu, B.; Wen, S. P.; Tian, W. J. Macromolecules 2009, 42, 4491–4499.

19 Zoombelt, A. P.; Gilot, J.; Wienk, M. A.; Janssen, R. A. J. Chem Mater 2009, 21, 1663–1669.

20 Baran, D.; Balan, A.; Celebi, S.; Esteban, B. M.; Neugebauer, H.; Sariciftci, N. S.; Toppare, L. Chem Mater 2010, 22, 2978–2987.

21 Ahmed, E.; Kim, F. S.; Xin, H.; Jenekhe, S. A. Macromolecules 2009, 42, 8615–8618.

22 Yue, W.; Zhao, Y.; Tian, H. K.; Song, D.; Xie, Z. Y.; Yan, D. H.; Geng, Y. H.; Wang, F. S. Macromolecules 2009, 42, 6510–6518.

23 Helgesen, M.; Gevorgyan, S. A.; Krebs, F. C.; Janssen, R. A. J. Chem Mater 2009, 21, 4669–4675.

24 Yuan, M. C.; Chiu, M. Y.; Liu, S. P.; Chen, C. M.; Wei, K. H. Macromolecules 2010, 43, 6936–6938.

25 Ando, S.; Nishida, J. I.; Tada, H.; Inoue, Y.; Tokito, S.; Yamashita, Y. J Am Chem Soc 2005, 127, 5336–5337.

26 Osaka, I.; Zhang, R.; Sauve, G.; Smilgies, D. M.; Kowalewski, T.; McCullough, R. D. J Am Chem Soc 2009, 131, 2521–2529.

27 Osaka, I.; Sauve, G.; Zhang, R.; Kowalewski, T.; McCullough, R. D. Adv Mater 2007, 19, 4160–4165.

28 Shi, Q. Q.; Fan, H. J.; Liu, Y.; Hu, W. P.; Li, Y. F.; Zhan, X. W. J Phys Chem C 2010, 114, 16843–16848.

29 Yang, M. A.; Peng, B.; Liu, B.; Zou, Y. P.; Zhou, K. C.; He, Y. H.; Pan, C. Y.; Li, Y. F. J Phys Chem C 2010, 114, 17989–17994.

30 Huo, L.; Guo, X.; Zhang, S.; Li, Y.; Hou, J. Macromolecules 2011, 44, 4035–4037.

31 Jung, I. H.; Yu, J.; Jeong, E.; Kim, J.; Kwon, S.; Kong, H.; Lee, K.; Woo, H. Y.; Shim, H. K. Chem Eur J 2010, 16, 3743–3752.

32 Lee, S. K.; Cho, J. M.; Goo, Y.; Shin, W. S.; Lee, J.-C.; Lee, W.-H.; Kang, I.-N.; Shim, H.-K.; Moon, S.-J. Chem Commun 2011, 47, 1791–1793.

33 Zhang, M. J.; Guo, X.; Li, Y. F. Adv Energ Mater 2011, 1, 557–560.

34 Higuchi, H.; Nakayama, T.; Koyama, H.; Ojima, J.; Wada, T.; Sasabe, H. Bull Chem Soc Jpn 1995, 68, 2363–2377.

35 Higuchi, H.; Yoshida, S.; Uraki, Y.; Ojima, J. Bull Chem Soc Jpn 1998, 71, 2229–2237.

36 Becke, A. D. J Chem Phys 1993, 98, 5648–5652.

37 Lee, C. T.; Yang, W. T.; Parr, R. G. Phys Rev B 1988, 87, 785–789.

38 Frisch, M. J.; Trucks, G. W.; Schlegel, H. B.; Scuseria, G. E.; Robb, M. A.; Cheeseman, J. R.; Scalmani, G.; Barone, V.; Mennucci, B.; Petersson, G. A.; Nakatsuji, H.; Caricato, M.; Li, X.; Hratchian, H. P.; Izmaylov, A. F.; Bloino, J.; Zheng, G.; Sonnenberg, J. L.; Hada, M.; Ehara, M.; Toyota, K.; Fukuda, R.; Hasegawa, J.; Ishida, M.; Nakajima, T.; Honda, Y.; Kitao, O.; Nakai, H.; Vreven, T.; Montgomery, J. A., Jr.; Peralta, J. E.; Ogliaro, F.; Bearpark, M.; Heyd, J. J.; Brothers, E.; Kudin, K. N.; Staroverov, V. N.; Kobayashi, R.; Normand, J.; Raghavachari, K.; Rendell, A.; Burant, J. C.; Iyengar, S. S.; Tomasi, J.; Cossi, M.; Rega, N.; Millam, J. M.; Klene, M.; Knox, J. E.; Cross, J. B.; Bakken, V.; Adamo, C.; Jaramillo, J.; Gomperts, R.; Stratmann, R. E.; Yazyev, O.; Austin, A. J.; Cammi, R.; Pomelli, C.; Ochterski, J. W.; Martin, R. L.; Morokuma, K.; Zakrzewski, V. G.; Voth, G. A.;

Salvador, P.; Dannenberg, J. J.; Dapprich, S.; Daniels, A. D.; Farkas, Ö.; Foresman, J. B.; V. Ortiz, J.; Cioslowski, J.; Fox, D. J. Gaussian 09, Revision A.1, Gaussian, Inc., Wallingford, CT, 2009.

39 Pomerantz, M.; Cheng, Y. Tetrahedron Lett 1999, 40, 3317–3320.

40 Shi, Q.; Fan, H.; Liu, Y.; Chen, J.; Ma, L.; Hu, W.; Shuai, Z.; Li, Y.; Zhan, X. Macromolecules 2011, 44, 4230–4240.

41 Tong, M. H.; Cho, S.; Rogers, J. T.; Schmidt, K.; Hsu, B. B. Y.; Moses, D.; Coffin, R. C.; Kramer, E. J.; Bazan, G. C.; Heeger, A. J. Adv Funct Mater 2010, 20, 3959–3965.

42 Pommerehne, J.; Vestweber, H.; Guss, W.; Mahrt, R. F.; Bassler, H.; Porsch, M.; Daub, J. Adv Mater 1995, 7, 551–554.

43 Liu, J.; Zhang, R.; Sauvé, G.; Kowalewski, T.; McCullough, R. D. J Am Chem Soc 2008, 130, 13167–13176.

44 Zhang, S. M.; Fan, H. J.; Liu, Y.; Zhao, G. J.; Li, Q. K.; Li, Y. F.; Zhan, X. W. J Polym Sci A: Polym Chem 2009, 47, 2843–2852.

45 He, Y. J.; Li, Y. F. Phys Chem Chem Phys 2011, 13, 1970–1983.

46 He, Y. J.; Zhao, G. J.; Peng, B.; Li, Y. F. Adv Funct Mater 2010, 20, 3383–3389.

47 Anthony, J. E.; Facchetti, A.; Heeney, M.; Marder, S. R.; Zhan, X. W. Adv Mater 2010, 22, 3876–3892.

48 Vacar, D.; Maniloff, E. S.; McBranch, D. W.; Heeger, A. J. Phys Rev B 1997, 56, 4573–4577.

49 Shaw, P. E.; Ruseckas, A.; Samuel, I. D. W. Adv Mater 2008, 20, 3516–3520.

50 Coffin, R. C.; Peet, J.; Rogers, J.; Bazan, G. C. Nat Chem 2009, 1, 657–661.